Early Radiometric Performance of Landsat-9 Thermal Infrared Sensor

Julia A. Barsi *[a], Matthew Montanaro [b], Kurtis L. Thome [c], Nina G. Raqueno [b], Simon Hook [d], Cody H. Anderson [e], Esad Micijevic [e]
[a] SSAI, NASA/GSFC Biospheric Sciences Laboratory, Greenbelt, MD, USA 20771; [b] Rochester Institute of Technology, Rochester, NY 14623; [c] NASA/GSFC Biospheric Sciences Laboratory, Greenbelt, MD, USA 20771; [d] NASA/Jet Propulsion Laboratory, Pasadena, CA 21109; [e] USGS/EROS ECCOE, Sioux Falls, SD, USA 57198

ABSTRACT

Landsat-9, launched on September 27, 2021, carries the Thermal Infrared Sensor (TIRS). The Landsat-9 TIRS is a close copy of the Landsat-8 TIRS instrument; it is a two spectral-band, pushbroom sensor with three Sensor Chip Assemblies (SCAs) that cover the 15-degree field-of-view. The primary radiometric change between the instruments is the addition of baffling in the Landsat-9 TIRS telescope to mitigate the stray light issue that has impacted the radiometric quality of Landsat-8 TIRS.

The on-orbit radiometric performance is monitored using the on-board variable temperature blackbody and views of deep space. Maneuvers to look at and around the moon have provided an assessment of the stray light. The absolute calibration is monitored by vicarious calibration techniques by teams at NASA/Jet Propulsion Lab and the Rochester Institute of Technology.

Landsat-9 completed a three-month commissioning phase in January 2022 and has been operational since February 2022. The instrument has demonstrated excellent radiometric performance, as assessed from the on-orbit measurements. The TIRS instrument is radiometrically stable to 0.1% within a power cycle, and has noise levels below 0.1K. The lunar scans and the vicarious calibration data provide evidence that the stray light has been effectively mitigated.

Keywords: Landsat-9, TIRS, thermal band, radiometric calibration

1. INTRODUCTION

The Thermal Infrared Sensor (TIRS), on board the Landsat-9 satellite, is the latest in the Landsat series of thermal imagers. Launched on September 27, 2021, the Landsat-9 TIRS instrument is a close copy of Landsat-8 TIRS; it is a pushbroom focal plane with two spectral bands in the long-wave infrared spectral region. Landsat-9 TIRS maintains continuity with previous Landsat instruments in its swath width, scene framing, and geometric accuracy and precision. The Landsat-8 and Landsat-9 spacecraft are orbiting in the same 705km orbit, with an 8-day offset in their revisit time. Both spacecraft include an Operational Land Imager on board, but this paper only details the radiometric performance of Landsat-9 TIRS since launch.

1.1 The Landsat-9 TIRS Instrument

TIRS is a pushbroom-design instrument with a focal plane that consists of three separate Sensor Chip Assemblies (SCAs), each 512 x 640 detectors to cover the 185km swath width (Figure 1) [Reuter, 2015]. The spectral interference filters each cover about 30 rows of detectors on each chip, though only select detectors are read for each band to generate the standard image product. The filters were designed to provide bandpasses suitable for use with a split-window atmospheric correction algorithm. The band-average spectral responses are shown in Figure 2.

* julia.barsi@nasa.gov; phone 1 301 614-6667

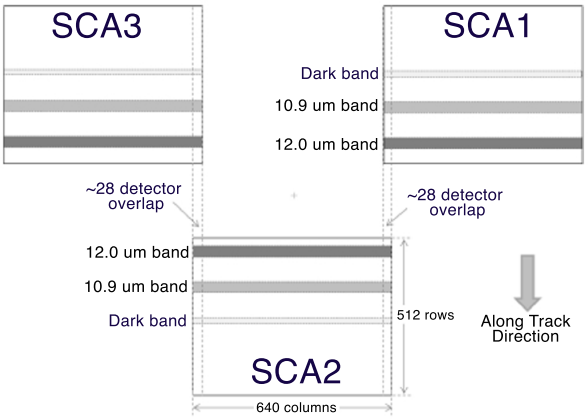

Figure 1. The focal plane design of the TIRS instruments. The 15° field-of-view is covered by three SCAs, each 512x640 arrays of Quantum Well Infrared Photodetectors (QWIP) detectors.

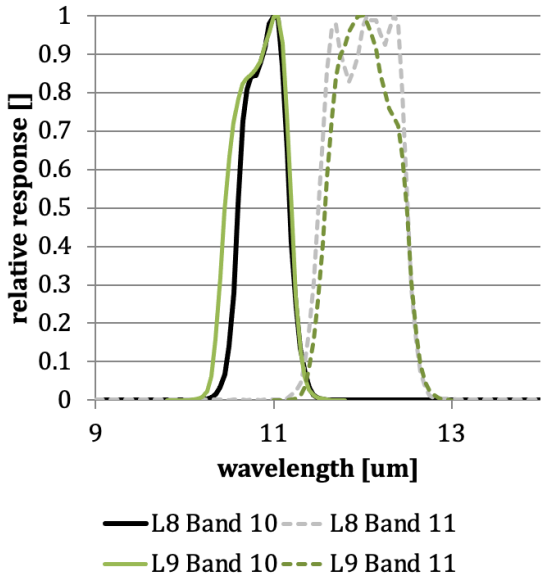

Figure 2. The spectral response of both Landsat-8 and Landsat-9 TIRS bands. The bandpasses were originally chosen to optimize a split-window atmospheric correction.

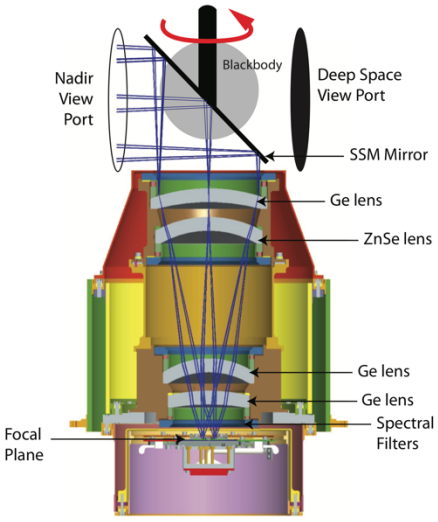

Figure 3. TIRS optical diagram. The SSM rotates between the nadir viewport, blackbody and deep space viewport to provide calibration data.

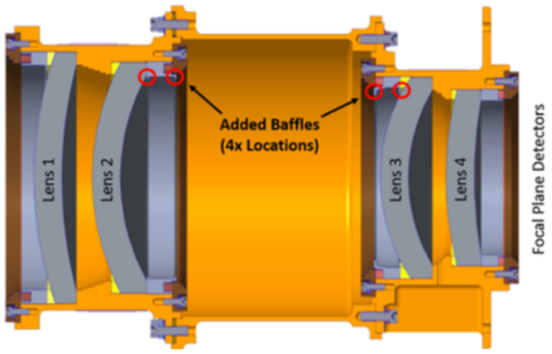

Figure 4. Cross-section of the Landsat-9 TIRS telescope indicating the locations of the new baffles meant to reduce the amount of scattering inside the telescope.

The instrument has a four-lens refractive optic telescope, with a mirror at the end of the telescope to change the view from the earth-viewing nadir port to the internal calibrator components (Figure 3). The Scene Select Mechanism (SSM) rotates between pointing at the nadir port, the internal blackbody and the deep-space view port.

1.2 Internal Calibration System

The blackbody and deep-space view constitute the internal calibration system. The variable temperature blackbody can be adjusted between 270 and 320K, though it is nominally kept at 295K. Twice an orbit, as the spacecraft is moving out of sunlight and just before it enters sunlight, TIRS images the blackbody and deep space port for regular characterization. Additional special calibration acquisitions are made periodically throughout the year for more complete characterization and calibration. This paper will focus on results from the data acquired at 295K.

2 STRAY LIGHT ARTIFACT

2.1 On Landsat-8 TIRS

Stray light was detected in the Landsat-8 TIRS imagery soon after launch. There was banding across the imagery that wasn't consistent from image to image and wasn't correctable using the normal on-board normalization tools. An on-orbit maneuver to scan the moon across an area thought to be outside the nominal field-of-view confirmed that energy from a zone about 13° off the optical axis was reaching the detectors [Montanaro, 2014]. This was later confirmed by high-fidelity optical modeling, which also revealed a weaker stray light feature from a zone about 22° off-axis. The reverse ray-trace modeling tracked the source of the stray light to reflections off the mounts that held lenses in place inside the telescope.

An algorithm was developed to remove the effect of the stray light in Landsat-8 TIRS data. It was implemented into the USGS processing system in 2016 and all Collection-1 and Collection-2 processed data include the correction for stray light.

2.2 Mitigation Efforts for Landsat-9 TIRS

The Landsat-9 TIRS telescope closely followed the design of the Landsat-8 TIRS telescope, though it included new baffles in front of the third lens to reduce the source of stray light (Figure 4). The Landsat-8 TIRS prelaunch tests for stray light were redesigned to more rigorously investigate possible stray light. Landsat-9 TIRS test measurements indicated that overall scattering was greatly reduced as compared to Landsat-8; the residual scattering at 13° was reduced from 0.4% on Landsat-8 TIRS to 0.03% in the Landsat-9 TIRS and from 0.024% to 0.01% for the 22° stray light feature [Montanaro, 2018]. The results from the prelaunch testing, along with the optical model, provided evidence that the total stray light would be greatly reduced, but there was still some uncertainty in the overall improvement due to the limited nature of the testing.

Once on-orbit, Landsat-9 performed an updated version of the lunar scans to verify the lack of stray light. The scans were tuned to establish that the magnitude and location of the stray light sources matched the prelaunch optical model. Figure 5 compares a sample of scattering from the 13° off-axis zone for Landsat-8 TIRS and Landsat-9 TIRS. In the Landsat-8 TIRS telescope, the worst-case scattering was ~0.4% (Figure 5, left). When the moon was in that same location during the Landsat-9 TIRS lunar scans, there was no discernable stray light (Figure 5, center). The worst-case stray light came from a smaller lobe at about 13°, which was predicted by the optical model, of <0.01% (Figure 5, right). The stray light from the zone about 22° off-axis was found to be 0.007%, as opposed to the 0.024% seen in Landsat-8 TIRS.

These on-orbit measurements clearly demonstrate the improvements in the Landsat-9 TIRS telescope. The magnitude of the stray light was reduced by more than ten times, and it was decided that the algorithm to correct the image products for stray light did not have to be applied to Landsat-9 TIRS data. Figure 6 illustrates the impact of the stray light correction algorithm for Landsat-8 and uncorrected image from Landsat-9.

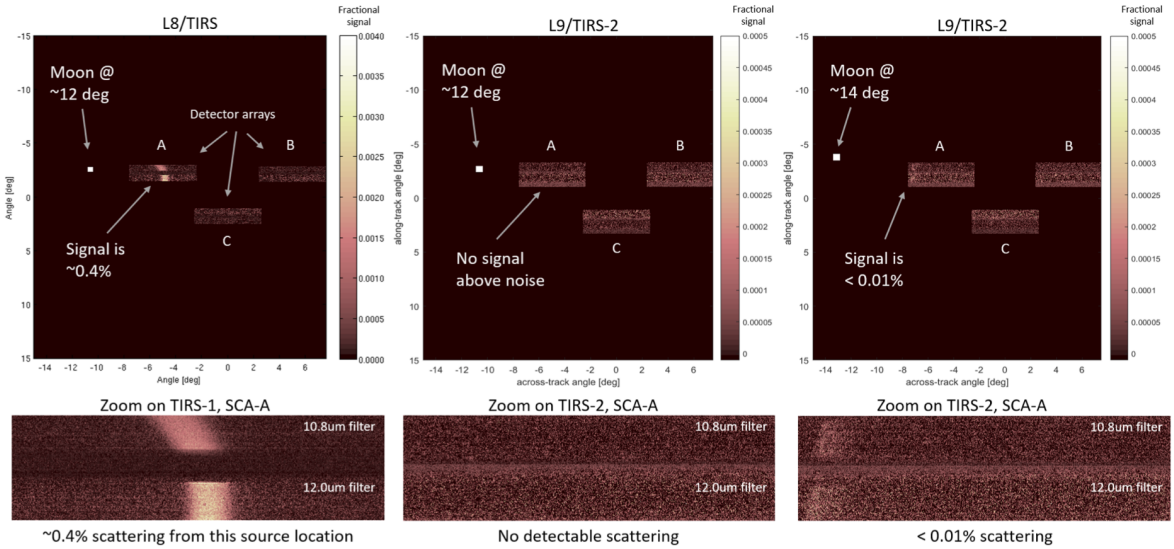

Figure 5. Image samples from the TIRS focal plane during the lunar scans. The top series of images shows the full TIRS focal plane for Landsat-8 TIRS (left) and Landsat-9 TIRS (center and right) for one lunar scan. The lower images show only one module, SCA-A. In the left-hand Landsat-8 TIRS sample, the moon is approximately 12° off-axis and there is a ghost of the moon in the SCA-A of about 0.4%. In the middle, moon is in the same location but in the Landsat-9 TIRS image, there is no discernable ghost. The moon is slightly further off-axis in the Landsat-9 TIRS image on the right, and there is a hint of the moon in SCA-A, but the total effect is less than 0.01%.

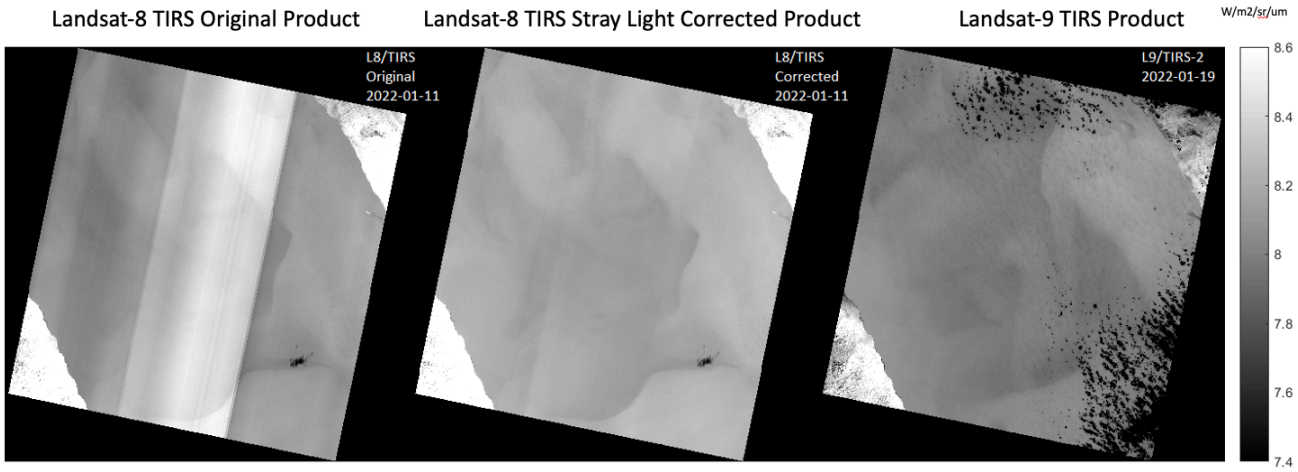

Figure 6. The stray light impacted the earth image data by creating banding, vertical nonuniformities, across the image, most obvious when looking large uniform areas, like this image of the Red Sea. On the left, the Landsat-8 TIRS image, which was processed without the stray light correction, the affect of the stray light is clear; there are vertical bands across the image that make the uniform water body appear very nonuniform. The center image shows the same Landsat-8 image, processed with the stray light correction algorithm; there are still artifacts of the stray light apparent, but it is much more uniform. The Landsat-9 TIRS image on the right is processed without the stray light correction; though the clouds make the image less uniform, there is no discernable trace of vertical banding.

3 ON-ORBIT RADIOMETRIC PERFORMANCE

Radiometric performance is monitored using regular observations of the internal calibration system. Here, the instrument stability and noise are evaluated by looking at the instrument response to the nominal 295K blackbody over time. Other on-orbit characterization using the special calibration collects can be found in [Pearlman, 2022].

3.1 Responsivity

The responsivity of the instrument is monitored by calculating an internal responsivity metric (r) from the paired acquisitions of blackbody and deep space:

$$r = \frac{(Q_{BB} - Q_{DS})}{(L_{BB} - L_{DS})} \quad (1)$$

where Q_{BB} is the instrument response to the blackbody, Q_{DS} is the instrument response to deep space, L_{BB} is the radiance of the internal blackbody as calculated from the thermistor on the blackbody and L_{DS} is the radiance of deep space (a 4K blackbody). The responsivity metric is calculated per-detector but only band-average metrics are presented here.

Prior to March 2022, the Landsat-9 TIRS instrument was stable to better than 0.05% in Band 10 and 0.2% in Band 11. On March 12, 2022, the TIRS Cryocooler Electronics (CCE) reset suddenly and resulted in the powering down of the instrument and loss of thermal control. After powering back on and once thermal control was recovered, the internal responsivity metric indicated that the response has changed by about 0.2% in both bands. The calibration parameters were updated using blackbody temperature sweep data [Pearlman, 2022].

This change in Landsat-9 TIRS responsivity is transparent to users of Level-1 and Level-2 products because the calibration parameters were updated.

After the CCE reset, the responsivity metric is stable to better than 0.05% in both bands over time. Figure 7 shows the responsivity change over time before the calibration parameter update (left) and the current calibration trend which considers that the calibration was updated at the CCE reset (right).

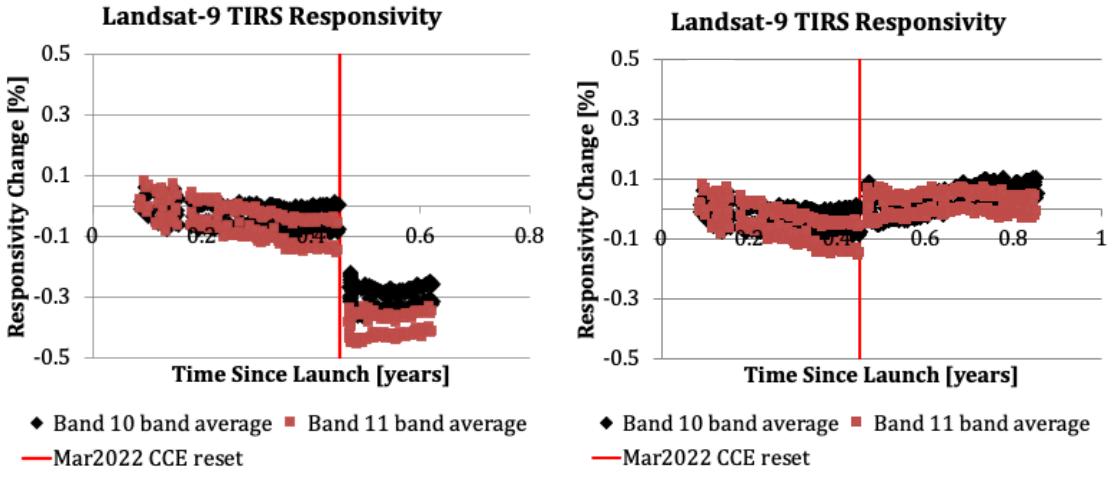

Figure 7. Responsivity change over time for both spectral bands of Landsat-9 TIRS. On the left, the trend indicates the magnitude of the change in responsivity after the CCE reset in March 2022, with trending through early May 2022. On the right, the trend has been revised to consider the updated calibration parameters. Both bands are stable to better than 0.05% since the CCE reset.

3.2 Response to Deep Space

The response to deep space is monitored overtime as an indicator of the stability of the instrument bias. Figure 8 shows the change in response to the deep space over time for both bands. There is a small level of drift, but it is within +/- 2DN (<0.2%). The March 2022 CCE reset appears to have reset the drift.

The instrument bias used by the processing system is calculated per orbit using the response to deep space.

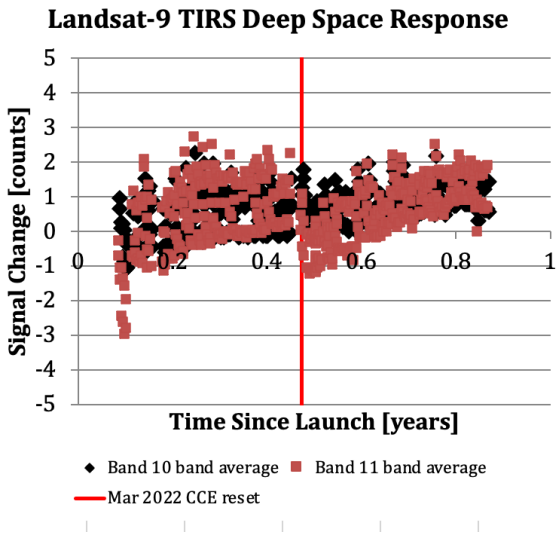

Figure 8. Change in reponse to deep space change over time for both spectral bands of Landsat-9 TIRS. There appears to be a slow drift over time that was reset at the CCE reset.

3.3 Noise Performance

The noise performance is tracked by modeling the Noise Equivalent Delta-Temperature (NEΔT) for five different temperatures using a subset of data acquired over one month of paired blackbody and deep space acquisitions (typically about 120 intervals total). The model is calculated per-detector to verify that there are no outliers. The median detector is trended over time to track stability.

For the period of July 2022, the NEΔT is better than 0.05K at 300K for Band 10 and 0.07K at 300K for Band 11 (Figure 9). The NEΔT is consistent to better than 1mK across all detectors in both bands. Figure 10 illustrates the stability of the median detector NEΔT over time. Both bands are stable to within 2mk since the start of nominal operations in Feb 2022.

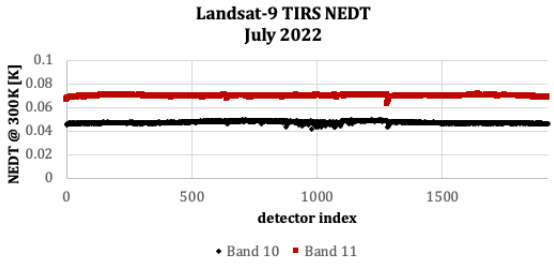

Figure 9. The modelled per-detector NEΔT at 300K for the month of July 2022. The Band 10 NEΔT is better than 0.05K and Band 11 is better than 0.07K for all detectors.

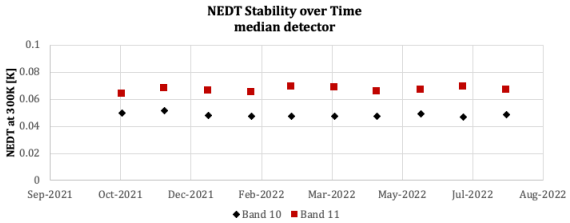

Figure 10. The modelled median detector's NEΔT at 300K over time. The NEΔT is stable to within 2mK (1-sigma) in both bands since the start of operations in Feb 2022.

3.4 Uniformity

In a pushbroom instrument with almost 2000 detectors across the focal plane in a single band, the per-detector normalization is an important step to minimizing visible stripes in the image products. The responsivity of individual detectors relative to the mean, also referred to as relative gains, are monitored using the blackbody data. It was found in Landsat-8 TIRS that the relative gains were changing slowly over time, but these changes were not being accounted for in the processing system. This resulted in an increasing level of striping, vertical nonuniformity due to individual detectors. The striping was getting worse over time. With the implementation of the Collection-2 processing system in 2020, the USGS added a quarterly calibration update to reduce striping in the Landsat-8 TIRS bands [USGS, 2021].

Though the relative gains of all detectors contribute to striping, the radiometric stability of individual detectors with specific change characteristics are flagged and are used as representative samples of detector performance. Individual detectors which display a relative responsivity that has changed by 0.5% or more in one transition are referred to as jumpers. Individual detectors which display a relative responsivity that has changed by 0.25% over time or more are referred to as drifters. Figure 11 is an example of two such detectors on Landsat-9 TIRS Band 10. Detector 944 exhibits several large jumps greater than 0.5%, while Detector 1127 is slowly changing over time with a cumulative change since launch of about 0.5% after about 0.45 years on orbit. The impact of both detectors' changes is small error in absolute calibration for this detector and a visible stripe in the image, if left uncorrected. To date, there have been 10 total jumpers in Landsat-9 TIRS and 12 total drifters.

The images of the blackbody are used to update the relative gains in the Calibration Parameter File on a quarterly basis. The average response of TIRS to the blackbody over the quarter is used to determine every detector's new relative gain; every detector gets a new relative gain every quarter. This means the effect of the changes in responsivity -- the jumpers and the drifters as well as the less significant responsivity changes -- should be corrected for in the image products within a quarter of the change occurring. Figure 12 shows a small subset of an image of a very uniform desert area; there are stripes visible in the June 20, 2022 image which are not apparent in the July 6, 2022 image due to the update of the relative gains on July 1, 2022. However, at least one new stripe has appeared between the image acquisition times; the responsivity of detector 944 (from Figure 11) increased by about 1% and results in a bright white stripe.

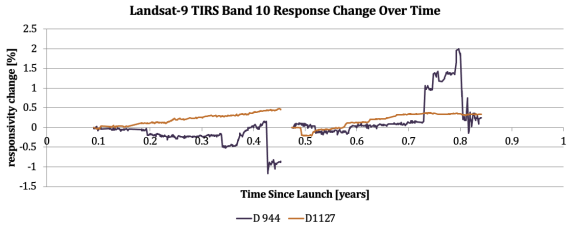

Figure 11. Plot illustrates the change in responsivity over time of two Landsat-9 Band 10 detectors. These two are representative of the jumper (sudden change of 0.5% or more) and drifter (slow cumulative change of 0.25% or more) behavior.

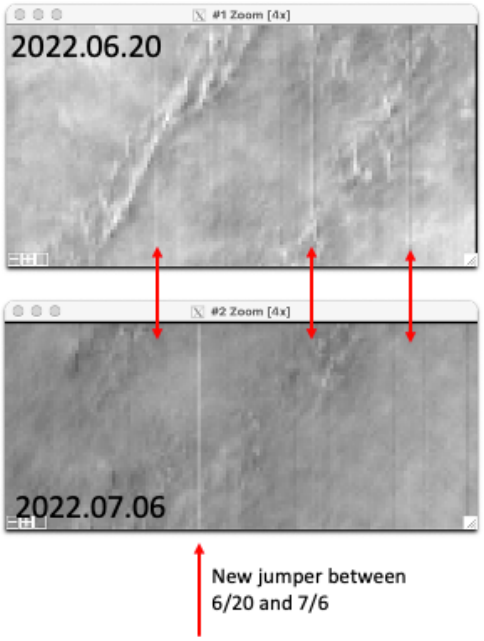

Figure 12. This pair of Landsat-9 TIRS Band 10 images illustrates the improvement in the uniformity across the image as a result of updating the relative gains, and the effect of jumpers. Both images are scaled to the same radiance range. The top image was acquired in June 2022, just before an update of the relative gains in the processing system. The bottom image was acquired in July 2002, just after the relative gain update. There are stripes apparent in this Level-1R detector-oriented image from June that have been corrected in the July image. However, one significant new stripe has appeared; the D944 responsivity jumped between the two images as is shown in Figure 11.

4 VICARIOUS CALIBRATION

The absolute calibration of the Landsat-9 TIRS is verified by vicarious calibration methods over large water bodies by two teams, one at NASA/Jet Propulsion Laboratory (JPL) and one at the Rochester Institute of Technology (RIT). Water is the ideal target for vicarious calibration in the thermal portion of the electromagnetic spectrum; it has well known and high emissivity, it is uniform in composition and it can exhibit low surface temperature variation over large areas. The JPL team operates a network of instrumented buoys on Lake Tahoe (CA/NV) and the Salton Sea. The typical range of temperatures covers 4-35C and both day and night data are used. The RIT team mines the data from the network of NOAA National Data Buoy Center buoys. The typical temperature range for the RIT data is 3-30C and only data acquired during the day are used.

The teams use different methods to get to surface-leaving radiance, but once they have estimated surface-leaving radiance (εL_T) from their measurements, they can compare top-of-atmosphere radiance (L_{TOA}) directly to the radiance reported by TIRS:

$$L_{TOA} = \varepsilon L_T \tau + L_u + L_d(1-\varepsilon)\tau \qquad (2)$$

where ε is emissivity [unitless], τ is the atmospheric transmission in the spectral bandpass [unitless], L_u is the upwelling radiance of the atmosphere, L_d is the downwelling transmission of the atmosphere and all radiances are in terms of [W/m^2 sr /μm]. The atmospheric parameters are generated by using radiance propagation code.

The Landsat-9 TIRS band-average absolute calibration is currently based on the prelaunch calibration [Pearlman, 2022] with an adjustment made for the 0.2% change in responsivity for data acquired after the March 2022 CCE reset (Figure 7). When comparing the vicarious water-based calibration to the instrument calibration, there is very good agreement. Figure 13 shows the 1:1 agreement between the top-of-atmosphere radiance predicted from the surface-leaving radiance and the radiance measured by TIRS. The difference between the two radiances is show in Figure 14. In both bands, there is a small indication of residual calibration error in offset; 0.16K in Band 10 and 0.61K in Band 11. The residual error from data acquired between Nov 2021 and April 2022 appears to be constant over time and is not dependent signal level. There does not appear to be any seasonal dependency, though this is still not a large dataset and does not yet cover a whole year. Both problems were present in the Landsat-8 TIRS vicarious calibration results and were likely an impact of the stray light.

The uncertainty of the vicarious calibration method has also gotten significantly better with the reduction in the stray light in the Landsat-9 TIRS telescope. The uncertainties are 0.3K for Band 10 and 0.5K in Band 11.

The residual errors reported by the vicarious calibration teams is based on a small dataset but are statistically significant. There has been no action to correct the radiometric calibration to date. If a calibration update is deemed necessary, it will likely be implemented in the USGS processing system in late 2022.

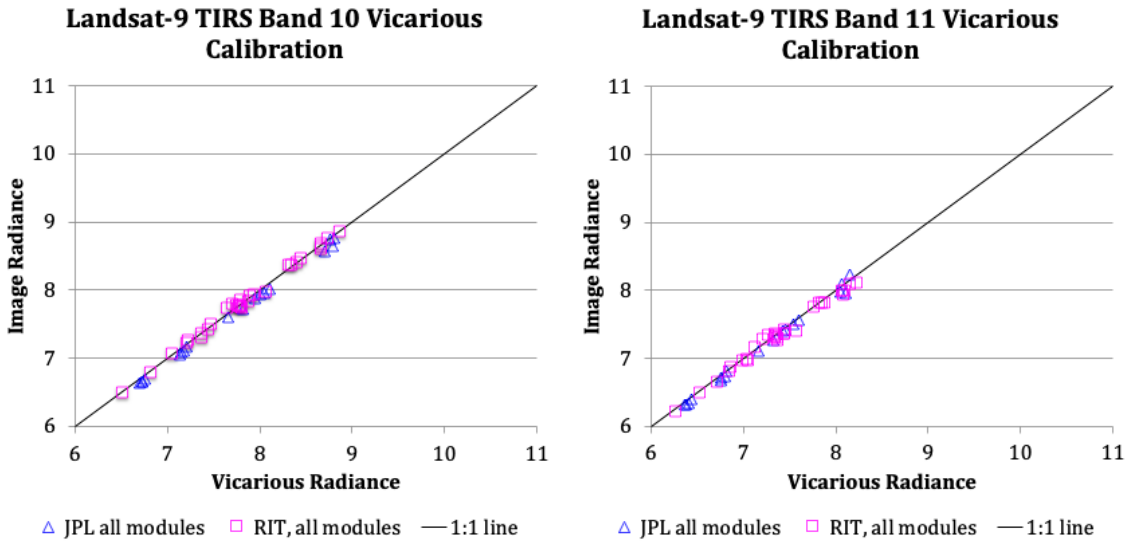

Figure 13. The collected vicarious calibration data from both JPL and RIT for Landsat-9, through April 2022. The comparison between the predicted top-of-atmosphere radiance and the image radiance is very good at this level. The data sit along the 1:1 line with very little scatter.

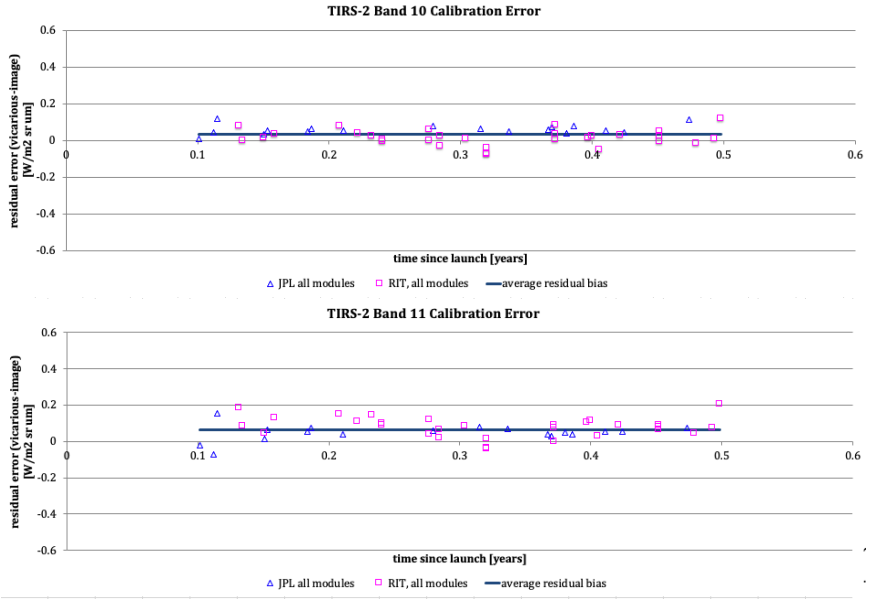

Figure 14. The residual radiometric calibration over time for data through April 2022. The average residual error for the whole dataset is plotted along with the individual RIT and JPL datapoints. The residual error appears to be independent of time and signal changes.

5 SUMMARY AND CONCLUSIONS

The Landsat-9 TIRS radiometric performance has been excellent to date. The stray light that affected the Landsat-8 TIRS radiometric accuracy was mitigated by baffles added to the telescope. The results from on-orbit lunar scans match the prelaunch tests for stray light. The overall impacts of stray light have been reduced by greater than 10 times.

The on-board calibrator system indicates that the instrument stability is better to 0.1% within a power cycle and the noise is better than 0.07K for both spectral bands.

The vicarious calibration results through April 2022 indicate there may be a small calibration error, of less than 0.2K in Band 10 and 0.65K in Band 11. The uncertainties for Landsat-9 are significantly better than the Landsat-8 TIRS uncertainties due to the reduction on the stray light.

REFERENCES

[1] NASA, "TIRS-2 Relative Spectral Response", Sept 2021, https://landsat.gsfc.nasa.gov/satellites/landsat-9/landsat-9-instruments/tirs-2-design/tirs-2-relative-spectral-response/

[2] Reuter, D.C.; Richardson, C.M.; Pellerano, F.A.; Irons, J.R.; Allen, R.G.; Anderson, M.; Jhabvala, M.D.; Lunsford, A.W.; Montanaro, M.; Smith, R.L.; Tesfaye, Z.; Thome, K.J. The Thermal Infrared Sensor (TIRS) on Landsat 8: Design Overview and Pre-Launch Characterization. *Remote Sens.* **2015**, *7*, 1135-1153. https://doi.org/10.3390/rs70101135

[3] Montanaro, M.; Gerace, A.; Lunsford, A.; Reuter, D. Stray Light Artifacts in Imagery from the Landsat 8 Thermal Infrared Sensor. *Remote Sens.* **2014**, *6*, 10435-10456. https://doi.org/10.3390/rs61110435

[4] M. Montanaro *et al.*, "Landsat 9 thermal infrared sensor 2 preliminary stray light assessment," in *Proc. IEEE Int. Geosci. Remote Sens. Symp. (IGARSS)*, Jul. 2018, pp. 8853–8856.

[5] USGS, "Landsat Collection 2 Level-1 Data," July 2021, https://www.usgs.gov/core-science-systems/nli/landsat/landsat-collection-2-level-1-data